Geophysical Research Letters

RESEARCH LETTER
10.1029/2024GL109352

Impacts of California Wildfires on CO_2 and Other Trace Gases

Thishan Dharshana Karandana Gamalathge[1], Nolan Tai[2,3], Xun Jiang[1], Xinyue Wang[1], Liming Li[4], and Yuk L. Yung[2]

[1]Department of Earth & Atmospheric Sciences, University of Houston, Houston, TX, USA, [2]Division of Geological and Planetary Sciences, California Institute of Technology, Pasadena, CA, USA, [3]Troy High School, Fullerton, CA, USA, [4]Department of Physics, University of Houston, Houston, TX, USA

Key Points:

- Increased CO_2, CO, and CH_4 levels during August-October (fire period) in California
- The underlying mechanisms for elevated concentrations of the trace gases differ for CO_2, CO, and CH_4
- Models simulate higher levels of CO_2 and CO but underestimate the observed enhancements, suggesting biases in the surface emissions and transports

Supporting Information:

Supporting Information may be found in the online version of this article.

Correspondence to:

X. Jiang,
xjiang7@uh.edu

Citation:

Karandana Gamalathge, T. D., Tai, N., Jiang, X., Wang, X., Li, L., & Yung, Y. L. (2024). Impacts of California wildfires on CO_2 and other trace gases. *Geophysical Research Letters*, *51*, e2024GL109352. https://doi.org/10.1029/2024GL109352

Received 23 AUG 2023
Accepted 22 SEP 2024

Author Contributions:

Conceptualization: Thishan Dharshana Karandana Gamalathge, Nolan Tai, Xun Jiang, Xinyue Wang
Data curation: Thishan Dharshana Karandana Gamalathge, Nolan Tai, Xun Jiang, Xinyue Wang
Formal analysis: Thishan Dharshana Karandana Gamalathge, Nolan Tai, Xun Jiang, Xinyue Wang
Funding acquisition: Xun Jiang
Investigation: Thishan Dharshana Karandana Gamalathge, Nolan Tai, Xun Jiang, Xinyue Wang
Methodology: Thishan Dharshana Karandana Gamalathge, Nolan Tai, Xun Jiang, Xinyue Wang

Abstract

Wildfires have broad impacts on the atmosphere, ecology, and society. This study leverages satellite data and chemistry-transport models to analyze the impact of wildfires on trace gases in California during the August-October periods of 2018, 2019, and 2020. During these months, Southern California experiences minimal precipitation, leading to a high Vapor Pressure Deficit, which results in decreased photosynthetic activities. This reduction, combined with increased biomass burning, causes a rise in CO_2 concentrations. Increased CO and CH_4 levels are also seen in TROPOMI retrievals tied to the increase in biomass burning. The CarbonTracker model captures these elevated CO_2 concentrations, though with a reduced amplitude of increased CO_2. Similarly, the GEOS-Chem model successfully simulates high CO levels but underestimates the observed enhancements. These findings will improve the understanding of fire's influence on trace gases and refine future numerical models on surface emissions and transport.

Plain Language Summary

The impacts of fires on trace gases (CO_2, CO, and CH_4) are examined from August to October in 2018, 2019, and 2020. During California's dry season, elevated concentrations of these trace gases are noted in satellite data, but the contributing mechanisms differ. CO concentrations primarily stem from biomass burning emissions, while CO_2 levels are affected by increased biomass burning and reduced photosynthetic activities. In contrast, CH_4 levels are impacted by both agriculture and biomass burning. These findings shed light on the complex relationship between fires and atmospheric trace gases, offering crucial insights to enhance future numerical models. A deeper understanding of the trace gas emissions from wildfires is also essential for assessing their impact on the climate system, air quality, and public health.

1. Introduction

With the wildfires in Hawaii, which mark one of the most devastating wildfire events in US history, biomass burning is receiving increasing attention. In addition to the huge societal damage, wildfires have significant impacts on the environment by destroying large areas of vegetation and releasing tremendous amounts of gaseous and particulate components into the atmosphere (Chin et al., 2002; Scholes & Andreae, 2000). For instance, there were 1910 fires (covering 2.73 million acres) from 1989 to 1998, whereas the period from 2009 to 2018 witnessed 3,356 fires (encompassing 7.08 million acres) in California alone (Buechi et al., 2021), suggesting a positive trend in California wildfires.

California is prone to enormous wildfires both in terms of intensity and frequency. Keeley and Syphard (2019) have found that wildfire's occurrence has significantly intensified in recent years. It reached an extreme level in 2017 and 2018, resulting in significant loss of life and property. The cost of fire suppression during these 2 years exceeded $1.5 billion, surpassing the previous 2 years (CalFire, 2018). It is also found that small fires and human-induced wildfires have increased rapidly in California over the past two decades (S. Li & Banerjee, 2021). While multiple factors contribute to wildfires, it has been shown that climate change is a critical factor for wildfires (e.g., Abatzoglou et al., 2019; Williams et al., 2019). For instance, periods of severe droughts, such as those in the decades of 1920–1930 and 1990–2020, have correlated with large amounts of area burned by massive fires in California (Keeley & Syphard, 2021).

Williams et al. (2019) offer valuable insights through a comparison of summer and fall wildfires in California. By analyzing California wildfires from 1972 to 2018, they found that the response of summer-burned areas to atmospheric vapor pressure deficit follows an exponential function. This implies that nearly all the summer forest

Resources: Thishan Dharshana Karandana Gamalathge, Nolan Tai, Xun Jiang, Xinyue Wang
Software: Thishan Dharshana Karandana Gamalathge, Nolan Tai, Xun Jiang, Xinyue Wang
Supervision: Xun Jiang
Validation: Thishan Dharshana Karandana Gamalathge, Nolan Tai, Xun Jiang, Xinyue Wang
Visualization: Thishan Dharshana Karandana Gamalathge, Nolan Tai, Xun Jiang, Xinyue Wang
Writing – original draft: Thishan Dharshana Karandana Gamalathge, Nolan Tai, Xun Jiang, Xinyue Wang
Writing – review & editing: Thishan Dharshana Karandana Gamalathge, Nolan Tai, Xun Jiang, Xinyue Wang, Liming Li, Yuk L. Yung

fires are driven by an increase in vapor pressure deficit. On the other hand, wind and low precipitation are the primary causes of wildfires during the fall season. The authors further argue that the underlying warming has amplified the potential for large wildfires in California.

The increase in biomass burning contributes significantly to the release of greenhouse gases (GHGs), such as CO_2 and CH_4, and pollutants like CO, which can affect atmospheric chemistry. The uptake of carbon by the biosphere can modulate CO_2 concentrations (Ahlström et al., 2015). While the terrestrial biosphere is considered a sink for atmospheric CO_2 (e.g., Poulter et al., 2014), it can also switch into a source of CO_2 during extreme conditions (Biederman et al., 2017; Jiang et al., 2021, 2023; A. X. Li et al., 2019). Therefore, monitoring surface CO_2 flux anomalies is crucial for understanding atmospheric CO_2 levels.

Although CO is not considered a greenhouse gas, it is classified as a pollutant harmful to public health and the environment. The dominant sources of CO are incomplete combustion from fuel and biomass burning (Worden et al., 2013). Bergamaschi et al. (2000) found that ∼25% of global CO is due to biomass burning. Fires in forests, shrublands, and peatlands produce more CO and other reduced trace gases (e.g., CH_4 and NH_3) because of significant smoldering compared to grass fires, where more efficient combustion occurs. For example, Africa is responsible for ∼72% of the total global burned area, yet produces only ∼44% of total global CO emissions (van der Werf et al., 2010). In contrast, Southeast and Equatorial Asia account for only 2.5% of the total burned area but contribute 22% of total global CO emissions (van der Werf et al., 2010). Furthermore, the 1–2 months lifetime makes CO a valuable tracer for studying tropospheric circulation, convection, and troposphere-stratosphere exchange (Pan et al., 1998).

In this paper, we will combine satellite data and numerical simulations to investigate the impact of California fires on trace gases (such as CO_2, CO, and CH_4). Column CO_2 from OCO-2, CO, CH_4, and Solar-Induced Fluorescence (SIF) from TROPOMI, the burned area from MODIS will be utilized in this study. In addition, CO_2 simulations from the NOAA CarbonTracker model and CO simulation from GEOS-Chem will also be employed in this paper to understand how realistic the models are in simulating the impact of fires on trace gases.

2. Data and Model

2.1. OCO-2 CO_2 Data

Orbiting Carbon Observatory—2 (OCO-2) measures reflected solar spectra, which can be used to infer atmospheric CO_2 levels. OCO-2 column-averaged dry air CO_2 (XCO_2) anomalies are particularly valuable for accessing extreme CO_2 flux anomalies (Feldman et al., 2023). Version 10 Column XCO_2 from OCO-2 with a good quality flag (Crisp et al., 2004, 2017) was used in this paper. OCO-2 CO_2 retrievals demonstrate consistency with surface column measurements, with an uncertainty of ∼1.5 ppm (Please refer to Wunch et al., 2017). We have regridded OCO-2 CO_2 data to a spatial resolution of 2° × 2°.

2.2. Burned Area Data From MODIS

The MODerate Resolution Imaging Spectroradiometer (MODIS) is aboard Terra and Aqua satellites, which complete 16 orbits per day in sun-synchronous orbits. MODIS serves as a valuable data source for various research applications. The MODIS sensor collects spectral data ranging 0.4–14.4 μm. It provides imaginary at a nominal resolution of 250, 500 m, and 1 km at nadir for different spectral bands (Giglio et al., 2018). Our study uses monthly mean MODIS burned area data with a spatial resolution of 0.25° × 0.25°.

2.3. SIF From TROPOMI

The TROPOspheric Monitoring Instrument (TROPOMI) is designed to measure CO and CH_4 among other atmospheric precursors. The ground pixel of TROPOMI is 7 km × 3.5 km at the nadir. TROPOMI spectra at 743–758 nm are used to estimate SIF (Kohler et al., 2018). A study by Turner et al. (2020) found that SIF measurements from TROPOMI agree with MODIS vegetation indices at annual time scales. TROPOMI SIF retrievals also demonstrate an excellent agreement with OCO-2 SIF retrievals. However, TROPOMI SIF has a better temporal and spatial resolution (Kohler et al., 2018). The TROPOMI SIF has a spatial resolution of 0.05° × 0.05°.

2.4. CO and CH_4 From TROPOMI

TROPOMI uses the shortwave infrared part of the spectrum (2,324–2,338 nm) to retrieve CO data (Landgraf et al., 2016) and shortwave infrared (2,305–2,385 nm) and near-infrared (757–774 nm) to retrieve CH_4 data (Veefkind et al., 2012). The initial spatial resolution is 7×7 km or 7×5.5 km, and we have regridded TROPOMI CO and CH_4 data to a spatial resolution of $0.5° \times 0.5°$. TROPOMI CO data agrees well with other satellite (MOPITT) and in-situ CO data with an uncertainty of ∼2 ppb (Martinez-Alonso et al., 2020). TROPOMI CH_4 agrees well with the TCCON CH_4 data with an uncertainty of ∼3 ppb (Lorente et al., 2021).

2.5. Model CO_2 From CarbonTracker

CarbonTracker is a global CO_2 model that monitors CO_2 sources and sinks, with a focus on North America. The CarbonTracker model (Jacobson et al., 2020) is used in exploring CO_2 in California. The CarbonTracker model uses Transport Model 5 to simulate advection, convection, and diffusion (Jacobson et al., 2020). The GFEDv4.1s database is linked with the biomass burning CO_2 emission calculations (Randerson et al., 2018), while the Carnegie-Ames Stanford Approach (CASA) model is used in calculating the biospheric CO_2 emissions (Potter et al., 1993). Satellite vegetation data, weather, and fire are considered in the CASA model to estimate CO_2 biospheric emissions (Giglio et al., 2006; Olsen & Randerson, 2004).

2.6. CO From GEOS-Chem

Goddard Earth Observing System (GEOS)—Chem is used to simulate CO. In the GEOS-Chem, GFED4 inventory is used for biomass burning. Community Emissions Data System version 2 (CEDS-v2) inventory is used as anthropogenic emission data. Data for biogenic emissions is through the Model of Emissions of Gases and Aerosols from Nature (MEGAN), while the Modern-Era Retrospective analysis for Research and Applications 2 (MERRA2) reanalysis data from NASA/GMAO is used as the input for the meteorological parameter.

2.7. Other Data Sets

Monthly mean precipitation data from Global Precipitation Climatology Project (GPCP) Version 2.3 data (Adler et al., 2018) are used in this paper. Monthly mean surface pressure, horizontal winds, and 500 hPa vertical pressure velocity from the National Centers for Environmental Prediction Reanalysis 2 (NCEP2) are used to explore the transport. Surface air temperature and relative humidity data from NCEP2 are used to estimate vapor pressure deficit (VPD) (Albright et al., 2022). The GPCP precipitation data and NCEP2 data are available over the global domain from January 1979 to the present. Quick Fire Emissions Dataset (QFED) CH_4 biomass burning emissions (Darmenov & da Silva, 2013) are used to analyze CH_4 surface emissions in different years. Daily CH_4 biomass burning emission data are available at $0.1° \times 0.1°$ (latitude × longitude), covering from February 2000 to the present.

3. Results

In this paper, we analyze the influence of wildfires on trace gases across California. August-October is chosen in this study, for it is the dry season in California and most wildfires occur during these months. We estimate the GPCP Version 2.3 precipitation over California during the period of August-October from 2018 to 2020 (Figure S1 in Supporting Information S1). Averaged precipitation in California during the period of August-October is about 7.7 mm/month in 2018, 8.7 mm/month in 2019, and 6.0 mm/month in 2020. Precipitation shows a strong north-south gradient. Precipitation is relatively high (∼15–20 mm/month) over the northern part of California, while it is very low (below 5 mm/month) over the southern part of California.

Associated with low precipitation (Figure S1 in Supporting Information S1), California has more fire activities during the dry season (August-October). MODIS burned areas averaged in each fire season (August-October of 2018, 2019, and 2020) are shown in Figure 1. Figure 1 illustrates significant fire activities in California and Nevada during the fire seasons, coinciding with the dry season. Fire events appear in both northern and southern California during August-October in 2018, 2019, and 2020. The total burned area over California during August-October is about 4.6×10^5 Ha in 2018, 1.3×10^5 Ha in 2019, and 14.4×10^5 Ha in 2020, which is much larger than the total burned area during the fire-inactive months (May-Jun) (0.6×10^5 Ha). Fire activities are relatively weak in August-October of 2019, medium in August-October of 2018, and the strongest in August-October of 2020.

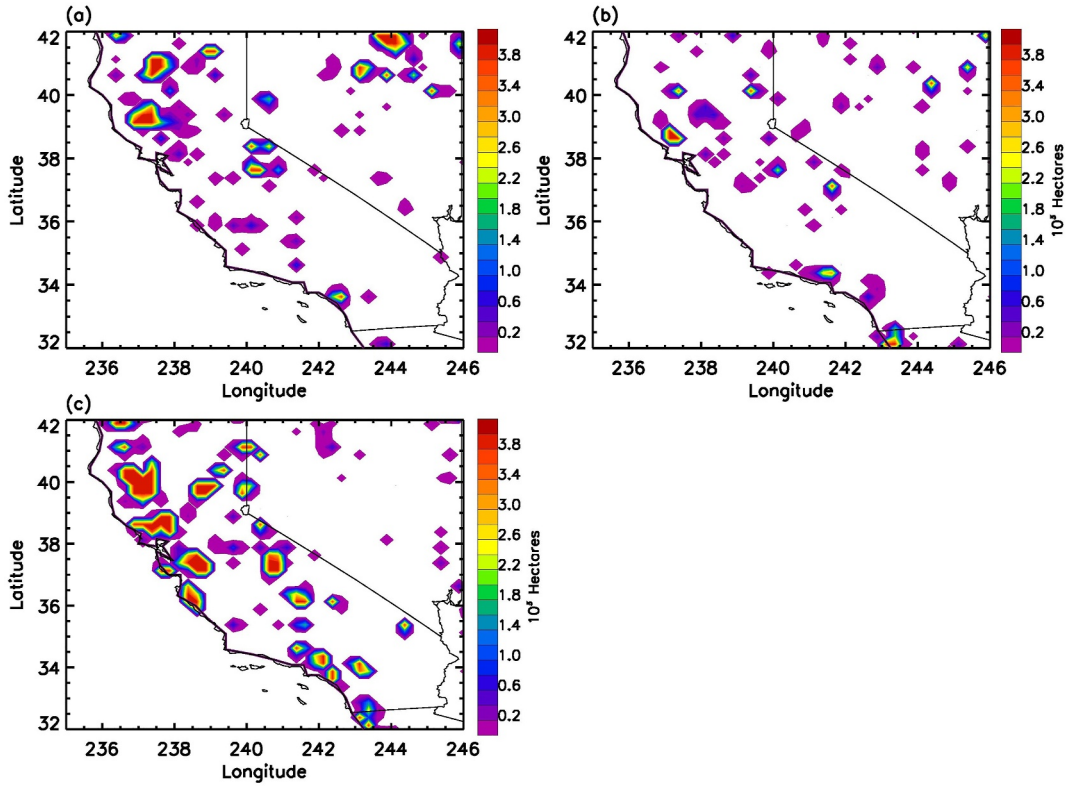

Figure 1. MODIS Burned Area in August-October of (a) 2018 (b) 2019 and (c) 2020. Units for burned area data are 10^3 Ha.

There are also more burned areas (fire activities) in August-October 2020 than in August-October of the previous 2 years (2018 and 2019). More fire activities will release more CO_2 into the atmosphere.

In addition to the precipitation, we calculate the VPD from NCEP2 Reanalysis data (Albright et al., 2022) in August-October of 2018, 2019, and 2020. VPD, defined as the difference between the saturation vapor pressure and the actual vapor pressure, is calculated from NCEP2 surface air temperature and relative humidity using Equation 1 in Barkhordarian et al. (2019). Results are shown in Figure S2 in Supporting Information S1. VPD can be used to represent how close the air is to saturation. High (low) VPD signifies that the air is more distanced from (closer to) saturation, indicating arid (humid) air. As shown in Figure S2 in Supporting Information S1, VPD demonstrates a west-east gradient. VPD has a lower value over western California, for the air is more humid in the coastal region. The average value of VPD during August-October is 20.9 hPa in 2018, 20.1 hPa in 2019, and 25.0 hPa in 2020 over California, which is higher than the VPD value in the non-fire months (10 hPa). VPD in California is higher in August-October 2020 than in August-October 2018 and August-October 2019, which means the air in California is dryer in August-October 2020. Low (high) VPD values are seen over northern (southern) California, which is related to the high (low) precipitation values over northern (southern) California. When the air is dry (high VPD, low precipitation), plants will close their stomata, suppressing the photosynthetic activities over southern California.

TROPOMI SIF is used to monitor the photosynthetic activities during the dry season (August-October) from 2018 to 2020. The results are shown in Figure S3 in Supporting Information S1. SIF values are low over most regions of California, with a slightly high SIF value over the northern part of California (where there are forests and agriculture), which is also related to the high value of precipitation (Figure S1 in Supporting Information S1) and low value of VPD (Figure S2 in Supporting Information S1) over those regions. TROPOMI SIF also demonstrates strong spatial variation, which is related to topography and central California agriculture activity. Averaged SIF values are 0.30, 0.36, and 0.28 $W/m^2/sr/\mu m$ over California in August-October of 2018, 2019, and 2020, respectively. During the dry season, there is less photosynthetic activity in California. SIF values are lower during August-October 2020 than the other 2 years, consistent with the lowest precipitation and highest VPD in August-October 2020. Lower SIF values in August-October 2020 also suggest less photosynthetic activity (less CO_2

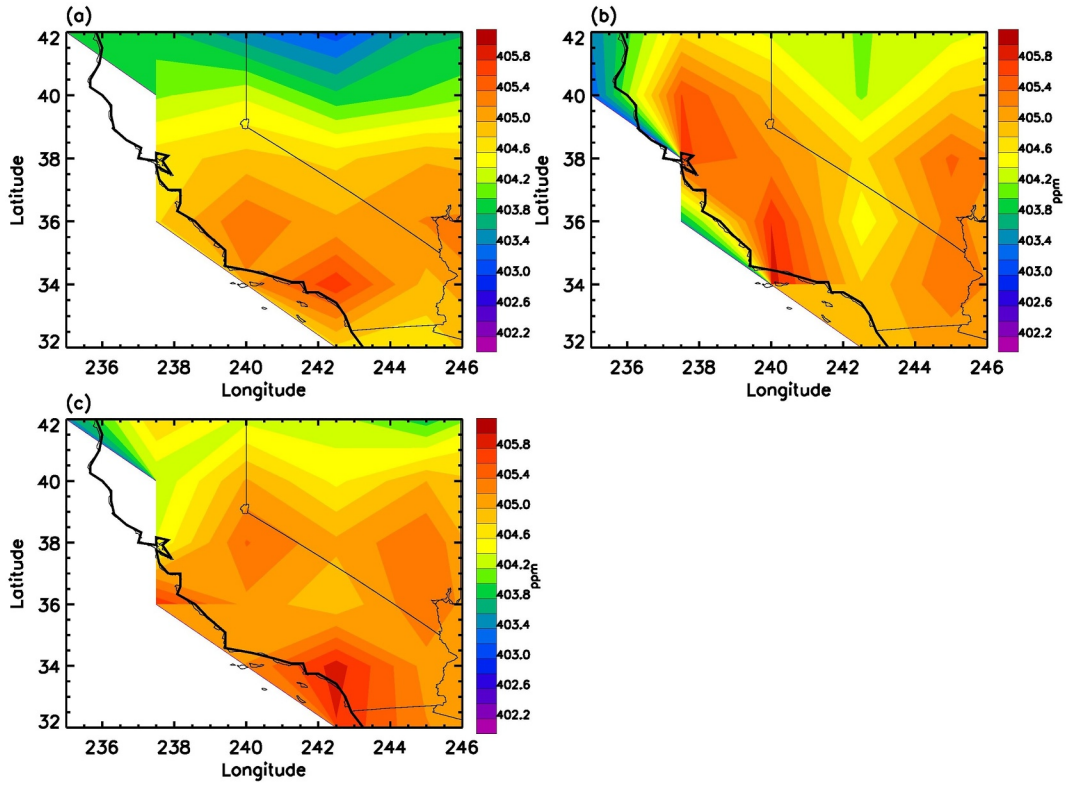

Figure 2. OCO-2 column-averaged CO_2 (XCO_2) data in August-October of (a) 2018 (b) 2019 and (c) 2020. Units for CO_2 data are ppm.

uptake from the biosphere) in 2020 than in the other 2 years, for the fire activities are strongest in 2020. Reduced photosynthetic activities during the dry season will remove less CO_2 from the atmosphere, which can lead to higher CO_2 concentrations in the atmosphere.

OCO-2 CO_2 averaged in August-October of 2018, 2019, and 2020 are shown in Figure 2. A linear trend has been extracted from the CO_2 data, allowing us to concentrate on the interannual fluctuations of CO_2 across different years. During the fire season (August-October), more CO_2 (1–2 ppm) is released into the atmosphere compared to the surrounding areas, which is attributed to intensified biomass burning and decreased photosynthesis within the same time frame. The average CO_2 during August-October in California is about 404.8 ppm in 2018, 404.9 ppm in 2019, and 405.1 ppm in 2020. Details of averaged CO_2 in California are summarized in Table S1 in Supporting Information S1. For each grid point in Figure 2, there are ~4,000 OCO-2 retrievals. The standard error for each CO_2 retrieval is 1.5 ppm (Wunch et al., 2017). Dividing 1.5 ppm by the square root of the number of retrievals, the error for CO_2 data in each grid point is less than 0.05 ppm. In August-October 2018, there is more CO_2 in central and southern California (Figure 2a), which is related to the biomass burning emission and reduced photosynthetic activity. At the same time, there is less CO_2 in the northern part of California, which is linked to heightened photosynthetic activities driven by increased precipitation and reduced VPD. High CO_2 values are observed across the entire California region in August-October 2019 and August-October 2020.

To evaluate the chemistry-transport model's ability to simulate elevated CO_2 levels over California during the dry season (August-October), we employ the CarbonTracker model to estimate CO_2 concentrations. We apply the OCO-2 CO_2 averaging kernel to the model's CO_2 vertical profile to get the convolved model CO_2. A linear trend is also extracted from the convolved model CO_2 to focus on interannual variations. Detrended and convolved CarbonTracker CO_2 in August-October of 2018, August-October of 2019, and August-October of 2020 are shown in Figure S4 in Supporting Information S1. The CarbonTracker model can capture high atmospheric CO_2 over California and Nevada, especially Southern California. In August-October 2018, the model demonstrates high CO_2 concentrations over the central and southern parts of California, similar to OCO-2 CO_2 retrievals (Figure 2a). In August-October 2019, model CO_2 is high over the majority region of California, similar to those from OCO-2

CO_2. However, there are some discrepancies between model CO_2 and OCO-2 CO_2 over the northern part of California. As shown in Figure S4c in Supporting Information S1, there is high CO_2 over the whole of California and Nevada, similar to the OCO-2 column CO_2 results in Figure 2c.

Figure S5 presents a scatter plot of OCO-2 CO_2 versus CarbonTracker model CO_2 (black symbols). While a linear relationship exists between these values, the CarbonTracker model underestimates CO_2. Scatter plots from the 2018, 2019, and 2020 dry seasons show slopes of 0.42, 0.26, and 0.31, respectively, indicating consistent underestimation. We also plot the difference between the OCO-2 CO_2 and CarbonTracker CO_2 in Figure S6 in Supporting Information S1 in the Supplementary Material. As shown in the spatial pattern of CO_2 difference (Figures S6g-6i in Supporting Information S1), the model CO_2 underestimates OCO-2 CO_2 over California. Possible causes for this discrepancy might include biases in surface emission inventories or weak vertical transport within the model simulation. In a sensitivity test, we have adjusted the CO_2 surface emission in the CarbonTracker. Results for the sensitivity test are shown as blue symbols in Figure S5 in Supporting Information S1. The slopes for the sensitivity simulation (blue symbols) have improved to 0.81, 0.42, and 0.56, respectively. The spatial distribution of adjusted CarbonTracker CO_2 is shown in Figures S6j-6l in Supporting Information S1. There are some improvements in the adjusted CarbonTracker CO_2, however, there are still discrepancies between adjusted CarbonTrack CO_2 and OCO-2 CO_2, which suggests that transports are also important in simulating CO_2. Since the CarbonTracker is an offline chemistry-transport model, we cannot explore the impact of transports on the model simulation. An interactive dynamical chemistry model is needed to understand the influence of transports on the CO_2 simulation in the future.

To further comprehend the impact of fires and the dry season on CO_2 levels, we also examine CarbonTracker surface CO_2 emissions from the biosphere and biomass burning. Biosphere CO_2 emissions are depicted in Figure S7 in Supporting Information S1. Biosphere CO_2 emission is defined as respiration minus photosynthesis. When the biosphere CO_2 emission is negative, there is more photosynthesis than respiration and the biosphere removes CO_2 from the atmosphere. In Central and Southern California, reduced photosynthetic activities result in reduced CO_2 uptake from the biosphere. Southern California experienced slightly higher CO_2 release in August-October 2020 compared to the same periods in previous years. In contrast, Northern California's high precipitation and low VPD promote extensive photosynthetic activities, facilitating the removal of CO_2 from the atmosphere. The averaged CO_2 uptake from the biosphere is -0.7×10^{-7}, -0.8×10^{-7}, and -0.4×10^{-7} mol m^{-2} s^{-1} for August-October of 2018, 2019, and 2020, with the largest reduction of biospheric CO_2 uptake in 2020.

CarbonTracker CO_2 emissions from biomass burning are displayed in Figure S8 in Supporting Information S1. The spatial patterns of CO_2 biomass burning emissions are similar to those from MODIS burned areas with California experiencing a substantial increase in biomass burning, particularly in the north. The averaged CO_2 biomass burning emissions are 0.6×10^{-7}, 0.2×10^{-7}, and 1.0×10^{-7} mol m^{-2} s^{-1} for August-October of 2018, 2019, and 2020, which is at least a factor of 10 increase compared with CO_2 biomass burning emission during the fire-inactive season (0.02×10^{-7} mol m^{-2} s^{-1}). The enhanced CO_2 absorption by the biosphere in Northern California (Figure S7 in Supporting Information S1) offsets the CO_2 emissions from biomass burning (Figure S8 in Supporting Information S1), explaining why OCO-2 column CO_2 concentrations are not significantly higher in the North compared to the South (see Figure 2).

NCEP2 surface pressure and horizontal winds are estimated for the periods of August-October in 2018, 2019, and 2020 (Figure S9 in Supporting Information S1). Low pressure is seen over Nevada and relatively high pressure over California. Winds blow from northern California to southern California, which will help to maintain high pollutants over southern California. We also calculate NCEP2 500 hPa vertical pressure velocity (dP/dt) over California (Figure S10 in Supporting Information S1). The positive (negative) value of vertical pressure velocity means sinking (rising) air. Sinking air is seen over California, which can trap pollutants in California.

With a lifetime of 1–2 months, CO is often used as a reliable tracer for biomass-burning emission estimates (Jiang et al., 2021; Yurganov et al., 2008). It is predominantly released during the smoldering phase (Andreae & Merlet, 2001). Figure 3 investigates the influence of fire on TROPOMI CO levels during August-October for the years 2018, 2019, and 2020. The average CO is 86 ppb over California in August-October 2018. Elevated CO concentrations are noticeable over Northern and Central California compared to Southern California in August-October 2018. The levels remain high in August-October 2019, averaging 84 ppb across California. In August-October 2020, CO concentrations rise to approximately 107 ppb (substantially higher than the other 2 years), attributable to increased fire activities (reflected by a larger burned area, 14.4×10^5 Ha) in 2020 compared to

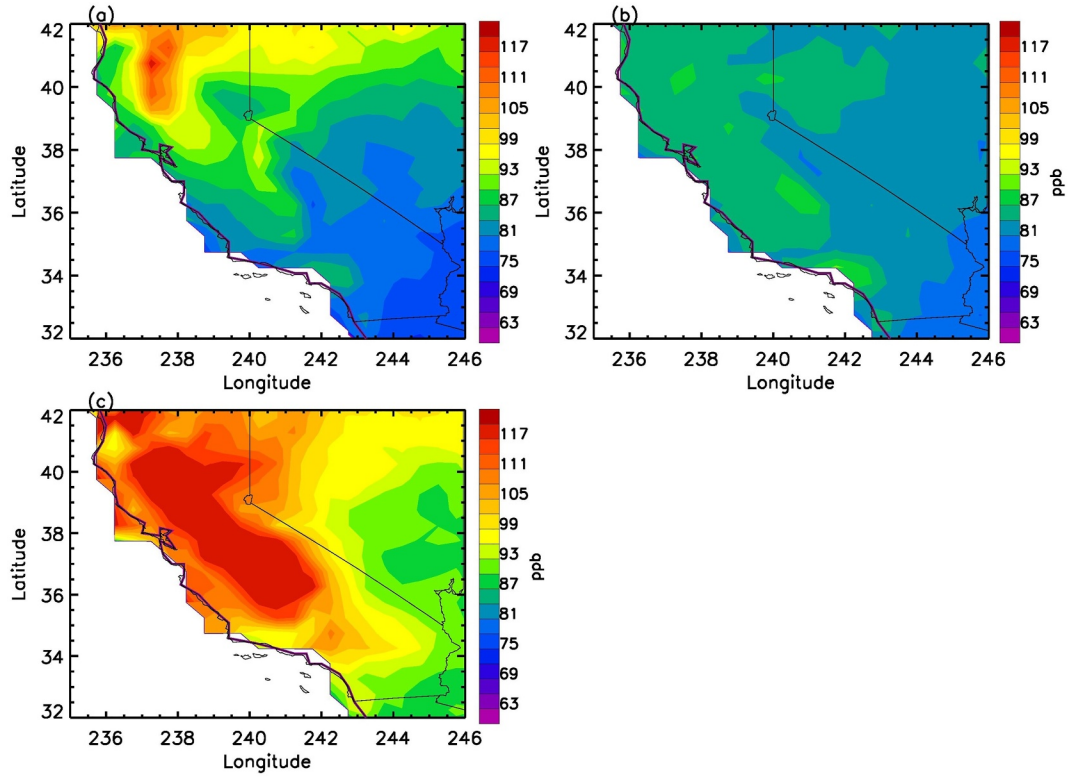

Figure 3. TROPOMI CO data in August-October of (a) 2018 (b) 2019 and (c) 2020. Units for CO data are ppb.

4.6×10^5 Ha in 2018 and 1.3×10^5 Ha in 2019, as shown in Figure 1. The TROPOMI CO averaging kernel is applied to the GEOS-Chem model's CO vertical profile. The resulting convolved model CO is depicted in Figure S11 in Supporting Information S1. Analogous to TROPOMI CO, higher GEOS-Chem CO concentrations are observed over Northern California in 2018, averaging 77.8 ppb. The GEOS-Chem model shows a low CO concentration of approximately 72.2 ppb in August-October 2019, which increases to around 79.1 ppb in August-October 2020. It should be noted that the GEOS-Chem model's CO concentrations are consistently lower than those indicated by TROPOMI over California. The underestimation of the CO level of GEOS-Chem might be attributed to the surface emission inventories and vertical transports in the GEOS-Chem.

Figure S12 in Supporting Information S1 presents a scatter plot comparing TROPOMI CO and GEOS-Chem model CO (black symbols) over California. In August-October 2018, the GEOS-Chem model accurately simulates Column CO with a slope of 0.97. However, it underestimates column CO in August-October 2019 and August-October 2020, with slopes of 0.60 and 0.44, respectively. Differences between TROPOMI CO and GEOS-Chem CO are shown in Figure S13 in Supporting Information S1. As shown in Figures S13g-13i in Supporting Information S1, GEOS-Chem model underestimates TROPOMI CO in most regions of California. In a sensitivity test, we have adjusted the CO biomass burning emission in the GEOS-Chem. The slopes of the sensitivity test (blue symbols) have improved to 0.99, 0.68, and 0.76, respectively. In Figure S14 in Supporting Information S1, we investigate CO biomass burning emissions from GFED4. Notably, high CO biomass burning emissions are observed over California, particularly in the north. Emissions are lower in August-October 2019 compared to August-October 2018 and August-October 2020, aligning with the GEOS-Chem model's CO results.

Ranked as the second most important greenhouse gas, CH_4 contributes considerably to climate forcing (IPCC, 2007). Biomass burning is an important source of methane. Therefore, we have also investigated TROPOMI CH_4 concentrations during California's dry season (August-October). These findings are presented in Figure S15 in Supporting Information S1. High CH_4 levels are observed throughout California during August-October across all 3 years, attributable to substantial CH_4 emissions from both biomass burning and agriculture. CH_4 concentrations are slightly higher in August-October 2020 (1862 ppb) than in 2018 (1855 ppb) and 2019 (1852 ppb). QFED CH_4 biomass burning emissions are estimated for August-October in 2018, 2019, and

2020 in Figure S16 in Supporting Information S1. This figure illustrates that both Northern and Southern California release CH_4 from biomass burning, with a greater source of CH_4 biomass burning in 2020 than in the preceding years. Over the 3 years, the highest CH_4 concentration is noted in Central California, primarily due to agricultural emissions, including livestock farming and croplands (Maasakkers et al., 2016).

4. Conclusion

The impacts of the California wildfire on CO_2, CO, and CH_4 are explored in this paper. For 2018, 2019, and 2020, the combined monthly averages of August-October are considered, for it corresponds to the dry season in California and exhibits the highest levels of fire activities. The average GPCP precipitation is low over California in August-October, with slightly high precipitation over the northern part of California and extremely low precipitation (<5 mm/month) over the southern part of California. Associated with low precipitation, the air is arid and further away from saturation (high VPD) in Southern California, reducing photosynthetic activities.

Total column CO_2, as retrieved by OCO-2, shows elevated CO_2 concentrations in California during the dry season (August-October). This aligns with MODIS data showing a large, burned area during August-October of 2018, 2019, and 2020. Relatively high precipitation is seen over northern California, while low precipitation is seen over southern California in August-October of 2018, 2019, and 2020 (Figure S1 in Supporting Information S1). During dry conditions (low precipitation), plants close the stomata, reducing the photosynthetic activity in southern California. As an indicator of photosynthetic activities, SIF values are high in northern California and low in southern California (Figure S3 in Supporting Information S1). In southern California, reduced photosynthetic activities reduce CO_2 uptake from the biosphere, leading to more CO_2 in the atmosphere (Figure S7 in Supporting Information S1). There is more burned area in northern California (Figure 1), which will release more CO_2 from the biomass burning to the atmosphere (Figure S8 in Supporting Information S1). The enhanced CO_2 emissions from biomass burning offsets the CO_2 absorption by the biosphere in northern California, explaining why column CO_2 concentrations are not significantly higher in the North compared to the South. Implementing the CarbonTracker model, developed to simulate CO_2 variability in California, indicates that nearly the entirety of California experienced high CO_2 levels during August-October of 2018, 2019, and 2020. The year 2020 saw the highest modeled CO_2 concentrations.

Given that CO is a reliable tracer for biomass burning, TROPOMI CO data also reveal high CO concentrations in California during the dry seasons (August-October) of 2018, 2019, and 2020, peaking in 2020. While the GEOS-Chem model can simulate high CO concentrations in California during these periods, it consistently estimates lower concentrations than TROPOMI CO. Alongside CO_2 and CO, it's also noteworthy that TROPOMI CH_4 concentrations are elevated across California during the dry season.

This study shed light on the impact of fires on trace gases, enhancing our understanding of the feedback cycle between wildfires and greenhouse gases (e.g., Fung et al., 2005; Jiang et al., 2023). It can also help us assess the potential impact of future wildfires on carbon budgets and climate trends. As highly effective greenhouse gases, CO_2 and CH_4 are critical in global warming. Understanding the emissions of these gases is crucial for assessing their contributions to the dynamic climate system. Furthermore, CH_4 and CO are detrimental gases with both immediate and long-term effects on air quality and public health. CH_4 can impact human health and air quality by serving as a precursor to tropospheric ozone (Mar et al., 2022). Analyzing the levels of the emission of these harmful gases (CH_4 and CO) from wildfires aids in the assessment of associated health risks. We anticipate that our investigations into these greenhouse gases (CO_2 and CH_4) can enhance our comprehension of climate change. Moreover, it's observed that numerical models tend to underestimate CO_2 and CO levels during August-October, which can be attributed to biases in surface emission inventories and transports in the models. The data gathered from satellite retrievals can be instrumental in refining and constraining these numerical models. While we focus on the southwestern part of the US, the insights gained from this study have broader relevance because wildfires are a global phenomenon. In the future, we will explore the impacts on trace gases before, during, and after fires, using geostationary satellite data with high spatial and temporal resolution as it becomes available.

Data Availability Statement

We downloaded OCO2 CO_2 data (Crisp et al., 2017) at https://disc.gsfc.nasa.gov/datasets?keywords=oco-2&page=1. TROPOMI data (Kohler et al., 2018; Landgraf et al., 2016; Veefkind et al., 2012) are from https://search.earthdata.nasa.gov/search?fi=TROPOMI. Precipitation data (Adler et al., 2018) are from https://psl.noaa.gov/data/gridded/data.gpcp.html. MODIS data (Giglio et al., 2018) are from http://modis-fire.umd.edu/.

Acknowledgments
This project is funded by NASA grant NNX16AG46G. We thank the anonymous referees and the editor for their time and constructive suggestions.

References

Abatzoglou, J. T., Williams, A. P., & Barbero, R. (2019). Global emergence of anthropogenic climate change in fire weather indices. *Geophysical Research Letters*, *46*(1), 326–336. https://doi.org/10.1029/2018GL080959

Adler, R. F., Sapiano, M., Huffman, G., Wang, J. J., Gu, G., Bolvin, D., et al. (2018). The Global Precipitation Climatology Project (GPCP) monthly analysis (new version 2.3) and a review of 2017 global precipitation. *Atmosphere*, *9*(4), 138. https://doi.org/10.3390/atmos9040138

Ahlström, A., Raupach, M. R., Schurgers, G., Smith, B., Arneth, A., Jung, M., et al. (2015). The dominant role of semi-arid ecosystems in the trend and variability of the land CO_2 sink. *Science*, *348*(6237), 895–900. https://doi.org/10.1002/2015JA021022

Albright, R., Corbett, A., Jiang, X., Creecy, E., Newman, S., Li, K. F., et al. (2022). Seasonal variations of solar-induced fluorescence, precipitation, and carbon dioxide over the Amazon. *Earth and Space Science*, *9*(1), e2021EA002078. https://doi.org/10.1029/2021EA002078

Andreae, M. O., & Merlet, P. (2001). Emission of trace gases and aerosols from biomass burning. *Global Biogeochemical Cycles*, *15*(4), 955–966. https://doi.org/10.1029/2000GB001382

Barkhordarian, A., Saatchi, S. S., Behrangi, A., Loikith, P. C., & Mechoso, C. R. (2019). A recent systematic increase in vapor pressure deficit over tropical south America. *Scientific Reports*, *9*(1), 15331. https://doi.org/10.1038/s41598-019-51857-8

Bergamaschi, P., Hein, R., Heimann, M., & Crutzen, P. J. (2000). Inverse modeling of the global CO cycle: 1. Inversion of CO mixing ratios. *Journal of Geophysical Research*, *105*(D2), 1909–1927. https://doi.org/10.1029/1999JD900818

Biederman, J. A., Scott, R. L., Bell, T. W., Bowling, D. R., Dore, S., Garatuza-Payan, J., et al. (2017). CO_2 exchange and evapotranspiration across dryland ecosystems of southwestern North America. *Global Change Biology*, *23*(10), 4204–4221. https://doi.org/10.1111/gcb.13686

Buechi, H., Weber, P., Heard, S., Cameron, D., & Plantinga, A. J. (2021). Long-term trends in wildfire damages in California. *International Journal of Wildland Fire*, *30*(10), 757–762. https://doi.org/10.1071/WF21024

CalFire. (2018). 2018 incident archive. Retrieved from http://www.fire.ca.gov/incidents/2018

Chin, M., Ginoux, P., Kinne, S., Torres, O., Holben, B. N., Duncan, B. N., et al. (2002). Tropospheric aerosol optical thickness from the GOCART model and comparisons with satellite and sun photometer measurements. *Journal Atmosphere Science*, *59*(3), 461–483. https://doi.org/10.1175/1520-0469(2002)059<0461:TAOTFT>2.0.CO;2

Crisp, D., Atlas, R. M., Breon, F. M., Brown, L. R., Burrows, J. P., Ciais, P., et al. (2004). The orbiting carbon observatory (OCO) mission. *Advances in Space Research*, *34*(4), 700–709. https://doi.org/10.1016/j.asr.2003.08.062

Crisp, D., Pollock, H. R., Rosenberg, R., Chapsky, L., Lee, R. A. M., Oyafuso, F. A., et al. (2017). The on-orbit performance of the Orbiting Carbon Observatory-2 (OCO-2) instrument and its radiometrically calibrated products. *Atmospheric Measurement Techniques*, *10*(1), 59–81. https://doi.org/10.5194/amt-10-59-2017

Darmenov, A., & da Silva, A. M. (2013). The quick fire emissions Dataset (QFED) – Documentation of versions 2.1, 2.2, and 2.4. *NASA TM-2013-104606*, *32*, 183. http://gmao.gsfc.nasa.gov/pubs/tm/

Feldman, A. F., Zhang, Z., Yoshida, Y., Chatterjee, A., & Poulter, B. (2023). Using Orbiting Carbon Observatory-2 (OCO-2) column CO_2 retrievals to rapidly detect and estimate biospheric surface carbon flux anomalies. *Atmospheric Chemistry and Physics*, *23*(2), 1545–1563. https://doi.org/10.5194/acp-23-1545-2023

Fung, I. Y., Doney, S. C., Lindsay, K., & John, J. (2005). Evolution of carbon sinks in a changing climate. *PNAS*, *102*(32), 11201–11206. https://doi.org/10.1073/pnas.0504949102

Giglio, L., Boschetti, L., Roy, D., Hoffmann, A. A., Humber, M., & Hall, J. V. (2018). Collection 6 MODIS burned area product user's guide. Version 1.2. Retrieved from http://modis-fire.umd.edu/files/MODIS_C6_BA_User_Guide_1.2.pdf

Giglio, L., van der Werf, G. R., Randerson, J. T., Collatz, G. J., & Kasibhatla, P. S. (2006). Global estimation of burned area using MODIS active fire observations. *Atmospheric Chemistry and Physics*, *6*(4), 957–974. https://doi.org/10.5194/acp-6-957-2006

IPCC. (2007). Summary for policymakers. In *Climate change 2007: Impacts, adaptation and vulnerability. Contribution of working group II to the fourth assessment report of the intergovernmental panel on climate change*. Cambridge University Press.

Jacobson, A. R., Schuldt, K. N., Miller, J. B., Oda, T., Tans, P., Mund, J., et al. (2020). CarbonTracker CT 2019B. *Global Monitoring Laboratory*. https://doi.org/10.25925/20201008

Jiang, X., Albright, R., Creecy, E., Li, K., Liang, M., Newman, S., et al. (2023). Congo basin rainforest is a net carbon source during the dry season. *Earth and Space Science*, *10*(2). https://doi.org/10.1029/2022EA002644

Jiang, X., Li, K., Liang, M., & Yung, Y. L. (2021). Impact of Amazonian fires on atmospheric CO_2. *Geophysical Research Letters*, *48*(5), e2020GL091875. https://doi.org/10.1029/2020GL091875

Keeley, J. E., & Syphard, A. D. (2021). Large California wildfires: 2020 fires in historical context. *Fire Ecology*, *17*(1), 22. https://doi.org/10.1186/s42408-021-00110-7

Keeley, J. E., & Syphard, S. D. (2019). Twenty-first century California, USA, wildfires: Fuel-dominated vs. wind-dominated fires. *Fire Ecology*, *15*(1), 24. https://doi.org/10.1186/s42408-019-0041-0

Kohler, P., Frankenberg, C., Magney, T. S., Guanter, L., Joiner, J., & Landgraf, J. (2018). Global retrievals of solar-induced chlorophyll fluorescence with TROPOMI: First results and intersensor comparison to OCO-2. *Geophysical Research Letters*, *45*(19), 10456–10463. https://doi.org/10.1029/2018GL079031

Landgraf, J., ann de Brugh, J., Scheepmaker, R., Borsdorff, T., Hu, H., Houweling, S., et al. (2016). Carbon monoxide total column retrievals from TROPOMI shortwave infrared measurements. *Atmospheric Measurement Techniques*, *9*(10), 4955–4975. https://doi.org/10.5194/amt-9-4955-2016

Li, A. X., Wang, Y., & Yung, Y. L. (2019). Inducing factors and impacts of the October 2017 California wildfires. *Earth and Space Science*, *6*(8), 1480–1488. https://doi.org/10.1029/2019EA000661

Li, S., & Banerjee, T. (2021). Spatial and temporal pattern of wildfires in California from 2000 to 2019. *Scientific Reports*, *11*(1), 8779. art. No. https://doi.org/10.1038/s41598-021-88131-9

Lorente, A., Borsdorff, T., Butz, A., Hasekamp, O., ann de Brugh, J., Schneider, A., et al. (2021). Methane retrieved from TROPOMI: Improvement of the data product and validation of the first 2 years of measurements. *Atmospheric Measurement Techniques*, *14*(1), 665–684. https://doi.org/10.5194/amt-14-665-2021

Maasakkers, J. D., Jacob, D. J., Sulprizio, M. P., Turner, A. J., Weitz, M., Wirth, T., et al. (2016). Gridded national inventory of U.S. Methane Emissions. *Environmental Science and Technology*, *50*(23), 13123–13133. https://doi.org/10.1021/acs.est.6b02878

Mar, K. A., Unger, C., Walderdorff, L., & Butler, T. (2022). Beyond CO_2 equivalence: The impacts of methane on climate, ecosystems, and health. *Environmental Science and Policy*, *134*, 127–136. https://doi.org/10.1016/j.envsci.2022.03.027

Martinez-Alonso, S., Deeter, M., Worden, H., Borsdorff, T., Aben, I., Commane, R., et al. (2020). 1.5 years of TROPOMI CO measurements: Comparisons to MOPITT and atom. *Atmospheric Measurement Techniques*, *13*(9), 4841–4864. https://doi.org/10.5194/amt-13-4841-2020

Olsen, S. C., & Randerson, J. T. (2004). Differences between surface and column atmospheric CO_2 and implications for carbon cycle research. *Journal of Geophysical Research*, *109*(D2), D02301. https://doi.org/10.1029/2003JD003968

Pan, L., Gille, J. C., Edwards, D. P., Bailey, P. L., & Rodgers, C. D. (1998). Retrieval of tropospheric carbon monoxide for the MOPITT experiment. *Journal of Geophysical Research*, *103*(D24), 32277–32290. https://doi.org/10.1029/98JD01828

Potter, C. S., Randerson, J. T., Field, C. B., Matson, P. A., Vitousek, P. M., Mooney, H. A., & Klooster, S. A. (1993). Terrestrial ecosystem production: A process model based on global satellite and surface data. *Global Biogeochemical Cycles*, *7*(4), 811–841. https://doi.org/10.1029/93gb02725

Poulter, B., Frank, D., Ciais, P., Myneni, R. B., Andela, N., Bi, J., et al. (2014). Contribution of semi-arid ecosystems to interannual variability of the global carbon cycle. *Nature*, *509*(7502), 600–603. https://doi.org/10.1038/nature13376

Randerson, J. T., van der Werf, G. R., Giglio, L., Collatz, G. J., & Kasibhatla, P. S. (2018). *Global fire emissions database, version 4.1 (GFEDv4)*. ORNL DAAC.

Scholes, M., & Andreae, M. O. (2000). Biogenic and pyrogenic emissions from Africa and their impact on the global atmosphere. *Ambio*, *29*(1), 23–29. https://doi.org/10.1579/0044-7447-29.1.23

Turner, A. J., Köhler, P., Magney, T. S., Frankenberg, C., Fung, I., & Cohen, R. C. (2020). A double peak in the seasonality of California's photosynthesis as observed from space. *Biogeosciences*, *17*(2), 405–422. https://doi.org/10.5194/bg-17-405-2020

van der Werf, G. R., Randerson, J. T., Giglio, L., Collatz, G. J., Mu, M., Kasibhatla, P. S., et al. (2010). Global fire emissions and the contribution of deforestation, savanna, forest, agricultural, and peat fires (1997–2009). *Atmospheric Chemistry and Physics*, *10*(23), 11707–11735. https://doi.org/10.5194/acp-10-11707-2010

Veefkind, J. P., Aben, I., McMullan, K., Förster, H., de Vries, J., Otter, G., et al. (2012). TROPOMI on the esa sentinel-5 precursor: A gmes mission for global observations of the atmospheric composition for climate, air quality and ozone layer applications. *Remote Sensing of Environment*, *120*, 70–83. https://doi.org/10.1016/j.rse.2011.09.027

Williams, A. P., Abatzoglou, J. T., Gershunov, A., Guzman-Morales, J., Bishop, D. A., Balch, J. D., & Lettenmaier, D. P. (2019). Observed impacts of anthropogenic climate change on wildfire in California. *Earth's Future*, *7*(8), 892–910. https://doi.org/10.1029/2019EF001210

Worden, H. M., Deeter, M. N., Frankenberg, C., George, M., Nichitiu, F., Worden, J., et al. (2013). Decadal record of satellite carbon monoxide observations. *Atmospheric Chemistry and Physics*, *13*(2), 837–850. https://doi.org/10.5194/acp-13-837-2013

Wunch, D., Wennberg, P. O., Osterman, G., Fisher, B., Naylor, B., Roehl, C. M., et al. (2017). Comparisons of the orbiting carbon observatory- 2 (OCO-2) XCO2 measurements with TCCON. *Atmospheric Measurement Techniques*, *10*(6), 2209–2238. https://doi.org/10.5194/amt-10-2209-2017

Yurganov, L. N., McMillan, W. W., Dzhola, A. V., Grechko, E. I., Jones, N. B., & van der Werf, G. R. (2008). Global AIRS and MOPITT CO measurements: Validation, comparison, and links to biomass burning variations and carbon cycle. *Journal of Geophysical Research*, *113*(D9). https://doi.org/10.1029/2007JD009229